arXiv:astro-ph/9808287v1 25 Aug 1998

Self-regulating galaxy formation as an explanation for the Tully-Fisher relation

D. Elizondo, G. Yepes
Departamento de Física Teórica C-XI, Universidad Autónoma de Madrid, Cantoblanco 28049, Madrid, Spain

R. Kates, V. Müller
Astrophysikalisches Institut Potsdam, Potsdam, Germany
and

A. Klypin
Department of Astronomy, New Mexico State University, Las Cruces, NM 88001

ABSTRACT

Using 3D hydrodynamical simulations of galaxy formation with supernova feedback and a multiphase medium, we derive theoretical relations analogous to the observed Tully-Fisher (TF) relations in various photometric bands. This paper examines the influence of self-regulation mechanisms including supernova feedback on galaxy luminosities and the TF relation in three cosmological scenarios (CDM, ΛCDM and BSI (broken scale invariance)). Technical questions such as dependence on resolution, galaxy finding algorithms, assignment procedure for circular velocity are critically examined.

The luminosity functions in the B and K bands are quite sensitive to supernova feedback at the faint end studied here. We find that the faint end of the B-band luminosity function ($-18 \leq M_B \leq -15$) is $\alpha \approx$ -(1.5 to 1.9). This slope is steeper than the Stromlo-APM estimate, but in rough agreement with the recent ESO Slice Project estimates.

The galaxy catalogs derived from our hydrodynamical simulations lead to an acceptably small scatter in the theoretical TF relation amounting to $\Delta M = 0.2 - 0.4$ in the I band, and increasing by 0.1 magnitude from the I-band to the B-band. Our results give strong evidence that the tightness of the TF relation cannot be attributed to supernova feedback alone. However, although eliminating supernova feedback hardly affects the scatter, it does influence the slope of the TF relation quite sensitively. With supernova feedback, $L \propto V_c^{3-3.5}$ (depending on the strength of supernova feedback). Without it, $L \propto V_c^2$ as predicted by the virial theorem with constant M/L.

The TF relation reflects the complex connection between depths of galaxy potential wells and the supply of gas for star formation. Hydrodynamic simulations provide direct information on this connection and its dependence on modeling parameters. Because of the small number of phenomenological parameters in our approach, it can serve as

a useful laboratory for testing various hypotheses and gaining insight into the physics responsible for the scatter, slope, and amplitude of the TF relation.

Subject headings: Hydrodynamics — Galaxies: formation, luminosity function — Methods: numerical

1. Introduction

The tight observed correlation between luminosity (L) and rotational velocity (V) of spiral galaxies, $L \propto V^{3.5-4}$, (Tully & Fisher, 1977; Pierce & Tully, 1988, 1992; hereafter TF relation) has proven to be one of the most useful tools in cosmology, most notably when applied to modeling of large-scale velocity fields and to the determination of the Hubble constant (see, e.g., Strauss & Willick, 1995). However, the TF relation is essentially empirical and has not yet received a comprehensive physical explanation within our current attempts to understand the mechanisms of galaxy formation and evolution. Although some relationship between luminosity and rotational velocity would certainly be expected from the virial theorem ($v^2 \propto GM/R$), the slope of the relation cannot be explained by a simply combining the virial theorem with a constant mass to luminosity assumption. Processes determining the luminosity of dark-matter halos must be an essential ingredient in any explanatory model. Hence, a key issue in understanding the origin of the TF relation is the effectiveness of star formation and its back-reaction on the galaxy formation process. A reliable theory of galaxy formation and evolution should be capable of answering the following questions: (i) why the relation has a small scatter; (ii) why the slopes and zero points are as observed; (iii) what additional variables (either potentially observable or hidden) could explain the residuals.

Different galaxies have different merging histories and different gas accretion rates. These processes affect star formation rates and hence could introduce scatter into the distribution of galaxy luminosities and colors. Thus the first question (low observed scatter) already represents a severe challenge for theory. Two mechanisms for explaining the low scatter were investigated by Eisenstein & Loeb (1996). First, one could suppose that galaxies formed prior to $z = 1$ and accreted only small amounts of material subsequently. However, neither the standard hierarchical clustering picture nor the particular simulations reported below support this hypothesis. Secondly, a strong feedback process could decouple the overall luminosity of spiral galaxies from details of their formation histories. This kind of mechanism is quite plausible, because it is known that dynamical systems with nonlinear feedback can be efficient at "forgetting" initial conditions and at reducing sensitivity to some parameters.

The second question (zero point and steepness of the slope) involves details of the star formation history within developing galaxies. Therefore, any realistic model of galaxy formation intending to answer this question needs to take into account at least the main physical mechanisms influencing the rate of star formation: gas dynamics and radiative processes.

Finally, the processes responsible for the explanation of the TF-relation involve variables (such as the merging and accretion history of the galaxy) that do not appear explicitly in the relation and which in this sense are "hidden" to the observer. A theoretical understanding, besides its importance as a basic scientific achievement, could offer several important practical advantages compared to a purely empirically-based relation: First, corrections to the relation on the basis of available observable properties could improve the accuracy of distance determinations. Second, the existence of possible systematic biases (such as hidden dependence on environment) is controversial (Pierce & Tully, 1988, 1992, Elizondo et al, 1998). If present, environmental bias in distance determination could have important consequences for mapping the large-scale velocity field. Third, if the form of the TF relation is sensitive to the model of structure formation, the relation could also be useful in discriminating among cosmological scenarios.

The analysis of Eisenstein and Loeb (1996) shows that the low scatter of the TF relation is unlikely to have resulted from initial conditions. This conclusion suggests that some regulation or feedback mechanism(s) must be at work. Whatever mechanism operates, it must keep both the mass-luminosity relation and the mass-velocity relation tight. Nonlinear processes that introduce feedback into galaxy formation include energy input and metal enrichment due to supernova explosions as well as hydrodynamics. All of these processes would be expected to contribute significantly to self-regulation of galaxy luminosities.

- Energy input by supernovae: The theory of the interstellar medium (McKee & Ostriker, 1977) implies that much of the energy of supernovae is converted to evaporation of cold clouds and thus has an important influence on subsequent star formation. The relative fraction of the energy used to evaporate clouds characterizes the degree of supernova feedback, as discussed below. In the context of galaxy formation and evolution, the feedback associated with injection of heat into the gas due to supernovae was

studied by Yepes, Kates, Khokhlov & Klypin (1997; YK^3) and found to have a significant self-regulating effect on the star formation history.

- Metal enrichment: During supernova explosions, metal enriched gas is distributed over large volumes within a galaxy and may even be transported to the intergalactic medium, in the case of small halos. Metals strongly increase the subsequent cooling rate, resulting in an increased star formation rate. Observationally, metallicity gradients in galaxies provide evidence for the effectiveness of this mechanism in the central regions of galaxies.

- Hydrodynamic feedback: The transport of gas depends on pressure gradients and thus it is particularly sensitive to the injection of large amounts of energy into the gas. Hence, in addition to the self-regulation due to cloud evaporation, there is also a strong self-regulating tendency due to gas flowing out of galaxies into lower-density regions, where the cooling time scale is longer. Gas which remains outside the galaxy will not contribute to further star formation inside the galaxy, and star formation from the gas fraction that does eventually fall back in will be delayed.

All those feedback mechanisms are tightly coupled, and it remains to be seen how such inherently complex processes can interact to yield relatively simple characteristics and relationships such as the TF relation.

The TF relation has been investigated using so-called "semi-analytical" models (Kauffmann et al., 1993 (KWG); Cole et al., 1994 (CAFNZ); Heyl et al., 1995 (HCFN), Avila-Reese, Firmani & Hernández 1998). Parametrising the merging history, gas cooling and star formation histories allows efficient generation of large synthetic galaxy data samples. The parameter space can then be investigated by testing the agreement with locally observed astrophysical processes. For example, semi-analytical models have been used for studying the influence of different cosmological evolution rates on galaxy formation processes. As a first step in understanding the processes involved in the TF relation, these investigations provide quite a bit of useful information.

As in the YK^3 model used here, the baryonic content of a halo in semi-analytic models (e.g. CAFNZ) typically consists of three components: hot gas, cold star-forming clouds, and stars. However, because gas dynamics are not explicitly simulated, the semi-analytical models require various uncontrolled assumptions such as specification of the shape of a halo. Generally, the models idealize a galaxy halo as a round object with an assumed density profile (typically an isothermal profile $\rho \propto r^{-2}$) and constant gas temperature (equal to the virial temperature). An assumed density profile is of course not necessarily even close to a solution of the gas dynamical equations. For example, during large mergers, it is neither possible to fit the density by a simple spherical density profile, nor may the gas be treated as isothermal. In particular, an understanding of environmental influence on galaxy properties (Elizondo et al., 1998) requires a hydrodynamic treatment, because gas flows are neither spherically symmetric nor confined to the interior of halos.

Since dynamical modeling is not included, semi-analytic models do not provide the flexibility of hydrodynamic simulations, which they often try to compensate for by involving extra fitting parameters. For example, as reported by HCFN, none of the models studied was able to reproduce the observed galaxy luminosity function and the TF relation simultaneously, even allowing the mass-to-light ratio to be a free parameter. It is possible to reconcile some of the discrepancies by neglecting star formation in halos with circular velocities greater than 500 km s^{-1}, as done by KWG, but this prescription was criticized by HCFN because it is preferable to avoid introducing ad hoc assumptions. HCFN also discussed the uncertainties associated with the identification of rotational velocities of galaxies with those of halos. Note that in the semi-analytical approaches, the gas is assumed isothermal out to the virial radius (radius of a sphere of overdensity 200), which as pointed out by HCFN may be violated. The scatter in the TF relation was reported by CAFNZ to be about 0.5 mag at 200 km s^{-1}, similar to the observed values, but with an increase in the scatter for low-velocity halos.

Hydrodynamical simulations of galaxy formation (e.g. Katz 1992; Cen & Ostriker 1992; Navarro & White 1994; Steinmetz & Müller 1994, Yepes et al. 1995, YK^3) offer the clear advantage of actually solving the gas dynamical equations. Hence, they can model the dynamical behavior of both the gas and the dark matter component at some level of accuracy in all conceivable situations, even when large mergers

occur. Nevertheless, they also have their own problems, such as limited resolution. This problem should gradually decrease in severity as computational costs fall. A more serious problem is that physical processes occurring far below the resolution limit, such as star-gas interactions, can have important effects and must therefore be included by hand. However, despite these problems, hydrodynamical approaches are a complementary tool to investigate the complex area of galaxy formation and to gain insight into the origin of the properties of galaxies we observe.

The structure of this paper is as follows: we start with a brief review of basic methodology we have used for studying the theoretical TF relation, including the model, simulation techniques, and galaxy identification schemes. Next we describe and critically discuss the assignment of rotational velocity to the *numerical* galaxies (§ 3). The fits to the luminosity-rotational velocity relation in the different color bands and their dependence on supernovae feedback are described in § 4. Section 5 is devoted to the study of the influence of numerical resolution and the galaxy finding algorithm on our results. In § 6 we show our estimates of the faint-end of luminosity functions in B and K bands and compare them with observational data. Finally, Section 7 is devoted to the discussion of results and conclusions.

2. Methods

2.1. Physical processes

To study the origin of the TF relation, we have used 3D gas dynamical simulations which include models for the most important physical processes in galaxy formation, as described in YK^3: these include gas dynamics, radiative and Compton cooling, star formation, star-gas interactions in the form of a two-phase approximation for the interstellar medium, and supernovae feedback. The universe is modeled as a 4-component medium consisting of dark matter, stars, "hot" or ambient gas, and cold clouds. Star formation is modeled by converting cold gas at a certain rate into discrete star particles. Each such event may be idealized as representing a small "starburst." Stellar population synthesis models (Bruzual & Charlot, 1993) are used to derive the luminosities and colors of the galaxies as a superposition of the starburst contributions.

The equations for the multifluid dynamics including star formation and supernova feedback, effects of resolution, and the values of "chemical" parameters were reported in detail in YK^3. Here we summarize the physical model in a slightly simplified form.

In each volume element, the amount of cold gas $m_{\rm cold}$ capable of producing stars is regulated by the mass of the hot gas $m_{\rm hot}$ that can cool on the time scale $t_{\rm cool}$, by the rate of forming new stable stars, and by the effects of supernova formation, which reheat and evaporate cold gas. The supernovae formation rate is assumed to be proportional to the mass of cold gas: $\dot{m}_{\rm SN} = \beta m_{\rm cold}/t_* \equiv m_{\rm SN}/t_*$, where $t_* = 10^8$ yr is the time scale for star formation, and β is the fraction of mass of newly formed stars that explode as supernovae ($\beta = 0.12$ for the Salpeter IMF). Each $1M_\odot$ of supernovae dumps $E_{SN} = 4.5 \times 10^{49}$ ergs of heat into the interstellar medium *and* evaporates a mass $A \cdot M_\odot$ of cold gas. The constant A will be referred to below as the "supernova feedback parameter" and is the most important parameter in the model.

The mass transfer between different components satisfies

$$\begin{aligned} \dot{m}_{\rm hot} &= \frac{A m_{\rm SN}}{t_*} - \frac{m_{\rm hot}}{t_{\rm cool}}, \\ \dot{m}_{\rm cold} &= -\frac{(m_{\rm cold} - m_{\rm SN})}{t_*} - \dot{m}_{\rm hot}, \\ t_{\rm cool} &= \frac{k T_{\rm hot} \mu m_H}{\rho_{\rm hot} \Lambda(T_{\rm hot}) C(\gamma - 1)}, \end{aligned} \qquad (1)$$

where k is the Boltzmann constant, T_{hot} is the temperature of the hot gas, μ is the molecular weight per particle, m_H is the mass of hydrogen, $\rho_{\rm hot}$ is the density of the hot gas, Λ is the cooling rate, and $\gamma = 5/3$ is the ratio of specific heats. The adjustable parameter $C = 1 - 10$ in the cooling time mimics the effects of unresolved substructure.

In the regime of active star formation, the main effects defining the temperature of the gas are supernova feedback and evaporation of the cold gas, which absorbs a significant fraction of the supernova energy:

$$m_{\rm hot} \dot{T}_{\rm hot} = \frac{m_{\rm SN}}{t_*} [T_{\rm SN} - A(T_{\rm hot} - T_{\rm cold})]. \qquad (2)$$

In this equation, $T_{\rm cold} \sim 10^4$K is the temperature of the cold gas, and $T_{\rm SN} = 1.1 \times 10^8$K is a measure of the energy released by a supernova: $kT_{\rm SN} = (\gamma - 1)\mu m_H \langle E_{\rm SN} \rangle / \langle m_{\rm SN} \rangle$. In order to mimic the effects of photoionization by quasars and AGNs, gas with overdensity less than 2 was kept at a constant

Table 1: Parameters of the scenarios

Parameters	CDM	ΛCDM	BSI
h	0.5	0.7	0.5
Ω_Λ	0	0.65	0
Ω_B	0.051	0.026	0.051
Ω_{dm}	0.949	0.324	0.949
rms fluctuation for $8h^{-1}$Mpc (σ_8)	1.2	1.0	0.6
Ω_{dm}	0.949	0.324	0.949
Simulation Box at $z = 0$, (Mpc)	5	5	5
Number of particles	128^3	128^3 (256^3)	128^3
Cell size at $z = 0$, (kpc)	39	39 (19.5)	39
Mass Resolution for dark matter ($10^6 M_\odot$)	4	2.7 (0.3)	4

(In brackets: parameters of the high-resolution simulation)

temperature of $10^{3.8}$K (Giroux & Shapiro, 1986; Petitjean, Mücket, & Kates, 1995). YK[3] found that results are relatively insensitive to the cooling enhancement factor C. For example, changing the factor from 1 to 10 gives practically the same results. This occurs because of the rapid increase in gas density after gravitational collapse sets in, leading to very effective cooling even for $C = 1$.

2.2. Overview of numerical simulations

The YK^3 code used here employs a combined N-body (PM) and hydrodynamic technique. The Eulerian hydrodynamical equations in the expanding Universe are solved on a grid using the *Piecewise Parabolic Method* (Colella and Woodward, 1984). The method includes high-resolution shock capturing technique and is capable of resolving hydrodynamic shocks without artificial viscosity.

In what follows, all quantities are expressed in physical units in which the Hubble constant of the corresponding cosmological scenario has been included (see Table 1).

A set of 11 simulations were first performed and analyzed for each of the cosmological scenarios used. This provides sufficiently large catalogs of "numerical galaxies" to allow statistically significant comparisons with observational quantities. These simulations were run using 128^3 particles on a 128^3 grid, both for the dark matter and the gas dynamics. We chose a box size of 5 Mpc as a compromise between the requirement of taking a representative part of the universe and having enough resolution to describe the mean star formation activity in a cell of the simulation volume. The cell size is thus 39 kpc, and the mass per particle is $\sim 4 \times 10^6 M_\odot$. The supernova feedback parameter in this simulation set was $A = 200$.

To study the effects of numerical resolution, we ran a test simulation for ΛCDM with the same box size and chemical parameters as the 11 realizations, but with 256^3 particles and cells (i.e. 19.5 kpc comoving and $3.3 \times 10^5 M_\odot$ mass per particle). We then reran this simulation at lower resolution (128^3 particles and cells). The initial particle distributions for all simulations were set up by the Zeldovich approximation. The displacement field used for the 128^3 grid was generated by a numerical average over the eight nearest cells of the displacement field in the 256^3 grid. This procedure allowed us to identify the same (massive) halos at the end of evolution in both simulations which made possible a reliable comparison of the effects of resolution in the final observational properties of the halo distribution. Increasing the resolution by a factor of two did not result in significant changes in global parameters (mass, luminosity) of bright galaxies. In particular no systematic change in the TF fit was found. Details and additional tests are reported in § 5.

To study the effects of supernovae feedback on the final observational properties of simulated galaxies, we repeated 6 of the 11 simulations for each cosmological model with the feedback parameter values $A = 50$ (strong gas reheating) and $A = 0$ (no reheating or mass transfer). Note, however, that we still keep metallicity enrichment in this case (see Table 2). A detailed discussion of the effects of supernova feedback on the TF relation is given in § 4.

The numerical code is parallelized to a degree of 95% for symmetric-multiprocessor computer architectures. All simulations reported here were performed in SGI Power Challenge and Origin 2000 supercomputers at the European Center for Parallelism in

Table 2: Number of galaxies in the simulations.

Model	Feedback Parameter	# realizations	# galaxies	# bright galaxies ($M_B < -16$)
CDM	A=200	11	447	73
	A=50	6	262	34
	A=0	6	288	77
ΛCDM	A=200	11	442	91
	A=50	6	260	33
	A=0	6	285	94
BSI	A=200	11	649	144
	A=50	6	318	36
	A=0	6	317	182

Barcelona (CEPBA).

2.3. Cosmological models

The parameters of the cosmological scenarios studied here are summarized in Table 1: We consider a standard CDM scenario, a low-density ΛCDM scenario, and a broken-scale-invariant (BSI) scenario which is based on a double inflation model. The BSI scenario was analyzed by Kates et al. (1995) using a particle-mesh code that included a thermodynamic model for the gas. The post-recombination power spectrum of the BSI model (for an analytic fit, see Kates et al., 1995) is similar to that of the τCDM scenario, in which the dark matter consists of a decaying neutrino.

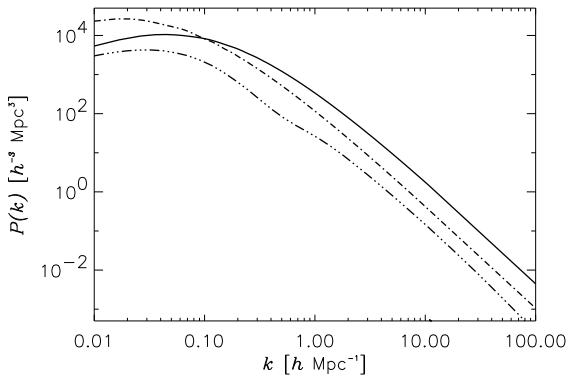

Fig. 1.— Initial power spectra for the CDM (solid), ΛCDM (dashed) and BSI (dash-dotted) models.

Within the simulated range of scales, the perturbation spectra for all three scenarios follow a power law, $P(k) \propto k^{-2}$. The power spectra for the three models are shown in Fig. 1. Although all three spectra are normalized to COBE, the spectral amplitudes differ considerably in our 5 Mpc box, because the normalization is performed on a scale much larger than the box. For example, the amplitude of the initial perturbations for BSI is about one-third that of CDM. That is, our BSI simulation can be considered as a CDM simulation with an effective normalization corresponding to $\sigma_8 = 0.35$. Hence, any inferences to be drawn should not be seen as statements about the viability of scenarios, but rather as a source of information on how the merging rate (CDM versus ΛCDM) or the time evolution (CDM versus BSI) influences the properties of galaxies. Our references to cosmological scenario dependence in what follows are to be understood with this caveat in mind.

2.4. Galaxy identification procedure

Galaxy identification poses difficulties in cosmological N-body simulations. Here we have at our disposal a substantial piece of information that is not available in pure dark matter simulations to distinguish galaxies among dark halos: the star (luminosity) distribution. In what follows, we use the term "galaxy" to refer to a halo with nonzero luminosity.

Our halo identification algorithm was given in YK[3] and is briefly reviewed here: We begin by looking for local dark matter density maxima with overdensity > 100 on the grid. We then define a sphere of radius 2 cells centered at the position of the maxima found. The position of the center-of-mass (CM) of all particles (dark+stars) within the sphere is then com-

puted. We then move the center of the sphere to the CM position and recompute the CM of the new particles lying within a sphere of the same radius. This procedure is iterated to convergence, which takes just a few iterations. In this way, we arrive to the true local maxima of the particle distribution. The total mass (baryons + dark matter) within the sphere is assigned as the mass for the halo. Now, if the mass within the sphere exceeds the mass corresponding to overdensity 200, we include this halo in our catalog. If the mass is lower, we repeat the algorithm with a sphere of radius 1 cell.

This procedure typically gives a radius and a mass for the halo that are well below the virial radius and close to the peak of the rotation curve, which is the area we are interested in. We have also checked that with this procedure, we avoid the problem of finding halos with substructures.

Using the stellar population synthesis model of Bruzual & Charlot (1993), we assign luminosities and colors to the galaxies (halos which have formed stars) by computing the spectral energy distribution (SED) according to

$$S(\lambda, t) = \sum_{\tau_i} \Phi(\tau_i) \mathcal{F}(\lambda, t - \tau_i), \qquad (3)$$

where $\Phi(\tau_i)$ is the mass of stars in the halo produced at timestep τ_i and $\mathcal{F}(\lambda, t)$ is the SED due to a starburst of 1 $M_\odot$ after an evolution time t. Convolving $S(\lambda, t)$ with the filter response function $R_f(\lambda)$, we obtain the absolute luminosity $L_f(t)$ in the given band. Combining the $L_f(t)$, we then obtain the evolution of the theoretical color index of the galaxy. (Of course, the color of a galaxy that would actually be measured will be influenced by other factors such as the interaction of starlight with the surrounding plasma.)

With this procedure, we typically obtain about a few tens of galaxy-like objects per simulation volume. In Table 2 we summarize the total number of galaxies found in all the simulations reported here. This number of galaxies permits statements concerning trends in the TF relation that are based on statistically significant estimates.

The 11 simulations carried out for each model correspond to a total simulated comoving volume of 1375 Mpc^3. Within this volume, we have also estimated the faint end of the galaxy luminosity function in the B and K bands and to compare these estimates with fits to the observational data, (see § 6).

In order to test the accuracy of the galaxy identification prescription, we have also used a somewhat more refined, but more computationally expensive algorithm in several of the simulations. The procedure is basically the same as above except that instead of computing quantities at fixed radius (1 or 2 cells), we compute the spherical mass and luminosity profiles. The radius is then increased until either the overdensity in the spherical shells falls below 200, or the radius touches a neighboring halo. This procedure begins with the highest-density maxima in order to define the large halos most reliably. We then define the *optical radius* (r_{opt}) of the halo, in analogy to observed galaxies, as the radius which contains ~ 80 % of the total light in the B band (Persic, Salucci & Stel 1996), assuming a pure exponential luminosity profile. The mass, circular velocity and luminosities for the galaxies correspond to the value of their respective radial profiles at r_{opt}.

The galaxies identified by these two procedures are the same, although their physical properties deviate slightly due to the different limiting radius of the halos. Nonetheless, the main results are not substantially modified.

3. Numerical estimates for the rotational velocity of galaxies

In observed spiral galaxies, circular disk velocities are inferred from spectroscopic linewidth estimates. Unfortunately, this procedure does not have a direct analog for our simulated galaxies: First, the numerical resolution of our simulations (39 kpc) does not allow us to assign a morphological type by identifying a disk structure inside halos. Second, at the limits of resolution, circular velocities estimated directly from the star particles in the simulations do not provide a realistic estimate of the "true" circular velocity.

To overcome the first difficulty, we assign a morphological type for galaxies based on their colors. As it turns out, most of the galaxies in our simulations are spirals, according to their position in the UBV color diagram (see Elizondo et al. 1998 for a more detailed discussion). This result is expected, because regions with high galaxy concentrations (groups and clusters of galaxies) are underrepresented due to the limited simulation box size.

To overcome the second difficulty, we have devised an operational procedure for assigning "rotational velocities" to our numerical galaxies. We have tested

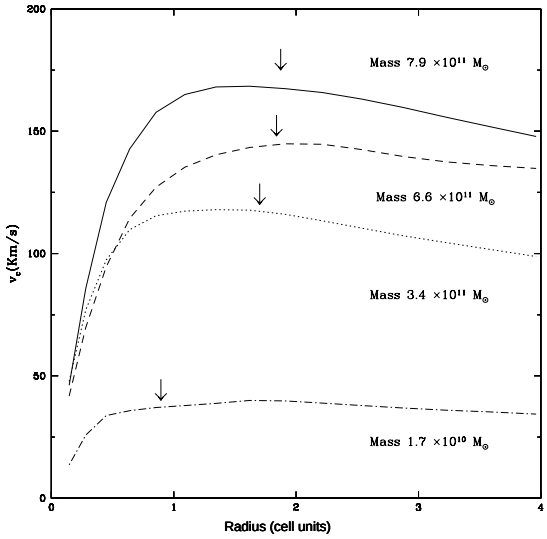

Fig. 2.— Circular velocity profiles for several halos of one of the ΛCDM simulations reported in the text. The circular velocity for the three more massive halos is assigned at 2 cell radii by our galaxy finding algorithm. For the less massive halo, velocity is assigned at 1 cell radii. The arrows indicate the corresponding value of $V_{2.2}$ for the different halos (see text).

this procedure for consistency in different ways. We define a gravitational (or circular) velocity, $v_{\rm grv} = \sqrt{GM/r}$, where M is the total mass (baryons+dark matter) of a galaxy within its assigned radius r of either 1 or 2 cells. To check whether our assignment of circular velocities at discrete radii is not introducing significant errors into the results, we have determined "circular velocity profiles" for a subsample of our numerical galaxies from their spherically averaged numerical density profiles. It turns out that $v_{\rm grv}$ nearly always coincides with the flat part of the rotation curve, as can be seen in Fig. 2, which means that our prescription for velocity assignment is reasonably accurate.

Even for real galaxies, different observational indicators for rotation velocities can be defined which yield different estimates of the TF relation. In a recent study, Courteau (1997) compares various measures of rotational velocity from optical rotation curves and linewidths in spiral galaxies. He concludes that the best estimate of the rotation velocity for TF applications, ($V_{2.2}$), is given at the location of peak rotational velocity of a pure exponential disk ($r_{disk} = 2.15h$, where in this context h is the disk scale length; see e.g. Freeman 1970). In order to check whether in the simulations our estimate of the circular velocity is compatible with the value of $V_{2.2}$, we have indicated it with an arrow in Fig 2. Assuming that the luminosity inside would follow an exponential disk profile, we can assign a characteristic disk scale length using $h = r_{opt}/3.2$. The estimate of r_{opt} is obtained by computing the radial luminosity profiles within the halos (see § 2.4). As can be seen in the figure, the values of $V_{2.2}$ are very close (within 5%) to the values of the circular velocity assigned by our algorithm.

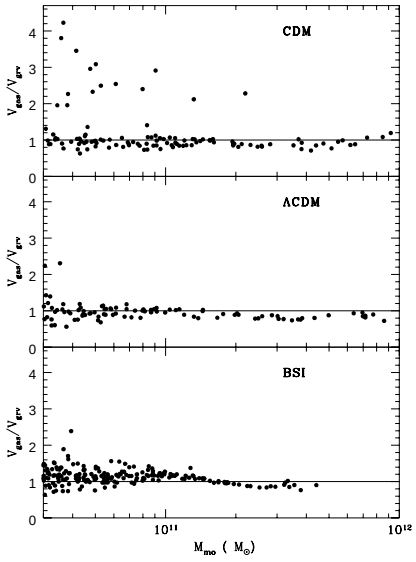

Fig. 3.— The ratio of the average gas velocity (estimated from the mass-weighted temperature) and the circular velocity of dark halos as a function of the mass of dark matter inside the halo (M_{mo}). The points close to a ratio of 1 represent galaxies in which the gas can be considered as an isothermal sphere.

As another test, we constructed an estimate of the rotational velocity using the gas velocity $v_{\rm gas}$. This estimate is based on the conjecture that the hot gas well follows the depth of the potential wells confining the dark matter halos and that the gas forms a rotationally supported disk. Therefore, the temperature of the gas should provide a good indicator for the circular velocity of the gas. To construct this indicator, we take the mass-weighted average of the tem-

perature, $< T >_M = \int \rho_{gas} T d^3x / M_{gas}$ to estimate the gas velocity assuming an isothermal distribution, $v_{\rm gas} = \sqrt{2k < T >_M / \mu m_p}$ (where m_p is the proton mass). The indicators $v_{\rm grv}$ and $v_{\rm gas}$ are compared for all three scenarios in Fig. 3. The agreement of the two indicators is typically quite remarkable. The only outliers to the tight relation between $v_{\rm grv}$ and $v_{\rm gas}$ are located in strongly interacting satellite galaxies, where the gas temperature is strongly influenced by the environment, possibly involving increased star formation and reheating due to supernova explosions. In these cases, $v_{\rm gas}$ would not be expected to provide a good indicator of the circular velocity. Most of these outliers are very faint, and hence they do not contribute to the fits to the magnitude-circular velocity relation, which as explained above included only galaxies with $M_B < -16$. Exclusion of those few outliers with $M_B < -16$ from the fits has only a minor effect in the results.

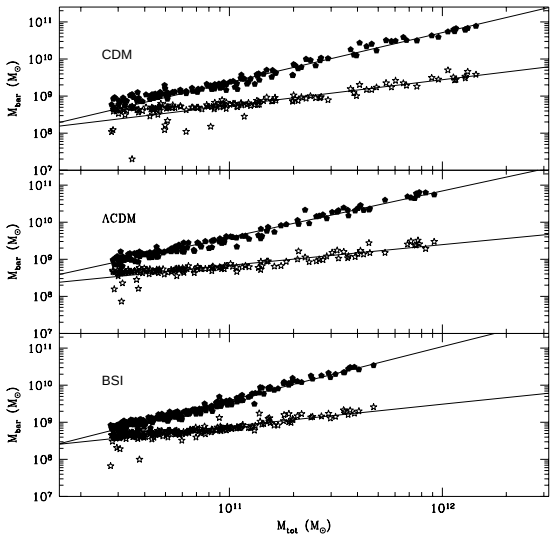

Fig. 4.— Relation between total mass and baryonic mass in the galactic halos used in the TF estimates ($M_B < -16$). Solid points represent the total mass in baryons (stars + gas) while starred symbols represent the total gas mass within the halo radius. Solid lines are the best fits to the points.

Incidentally, most of the outliers arose in CDM realizations. As is plausible from the CDM spectrum (Fig. 1), the advanced stage of evolution reached in the CDM model leads to more interacting faint galaxies than in the other models.

We have also performed a further check on our assignment of rotation velocities to galaxies. High-resolution hydrodynamical simulations have found a tight correlation between baryonic mass and maximum rotation velocity of the gas, $M_{bar} \propto V_c^{2.5}$ (Evrard, Summers & Davis, 1994). On the other hand, we obtain a very tight correlation between baryonic (gas + stars) mass and total mass in our halos. In Fig. 4 we plot this relation for the bright ($M_B \leq -16$) halos found in the simulations of the three different models. The best fits to this relation give quite similar results for CDM and ΛCDM ($M_{bar} \propto M_{tot}^{1.3-1.25}$). For the less evolved BSI model, where no big galaxies have been formed up to the present epoch, we find a slightly steeper slope ($M_{bar} \propto M_{tot}^{1.45}$). We also find a tight correlation between the total mass and the gas content in the halos. In this case, the correlation is pretty much the same for the three models, $M_{gas} \propto M_{tot}^{0.6}$.

We can now use the correlation found by Evrard, Summers and Davis (1994) together with the correlation between total mass and baryonic mass found in our simulations to obtain an independent relation between total mass and maximum circular velocity for the halos. Doing so yields $M_{tot} \propto V_c^{1.8-1.9}$, which is very close to the relation we have used ($M_{tot} \propto V_c^2$). Although this argument does not yield normalization constants, it provides clear evidence that at least the slope and the scatter of the TF relation computed from our simulations do not depend on the approximate estimate of the circular velocity.

Further tests concerning the effects of numerical resolution and galaxy finding algorithms on the determination of circular velocities of galaxies will be discussed in § 5.

4. Fits to the TF relation

From our galaxy samples in each scenario, we have computed magnitudes in the B, R, and I bands using the procedure of § 2.4. Figs. 5, 6 and 7 are plots of the B and I band magnitudes vs. circular velocity for the simulated galaxies in each of the three scenarios and for the three different feedback parameter values considered: $A = 200$ (realizations where the evaporation of cold clouds is the most important effect), $A = 50$ (realizations in which supernovae are very efficient at reheating the gas) and no supernova feedback (i.e. $A = \beta = 0$). All galaxies are plotted,

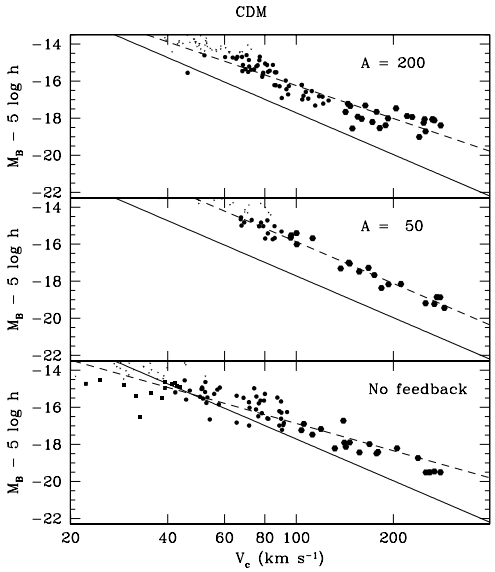

Fig. 5.— (a). The TF relation for the B band for galaxies found in CDM simulations with different feedback parameter values. The upper panel ($A = 200$) corresponds to simulations in which evaporation of cold clouds is the most important effect. The middle panel, ($A = 50$) correspond to simulations in which supernovae are very efficient at reheating the gas, but not evaporating the cold clouds. The lower panel correspond to the same simulations run without assuming any supernova feedback process ($\beta = 0$ see text.). Note, however, that we still kept metallicity enrichment in this case. The solid line shows the fit to the Tully-Fisher relation as determined by Pierce & Tully (1992). The dashed line is the best fit obtained by considering only simulated galaxies with $M_B < -16$. Black dots represent bright galactic galaxies ($M_B < -16$). Small crosses represent the faint galaxies found by our galaxy finding algorithm that were not taken into account in the fit.

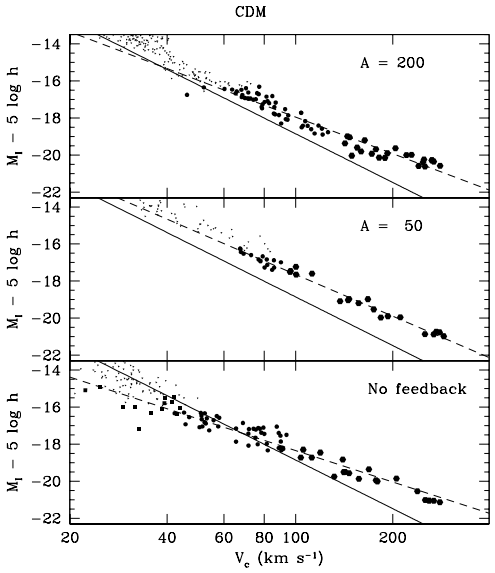

Fig. 5.— (b) Same as Fig 5.(a) for the I band

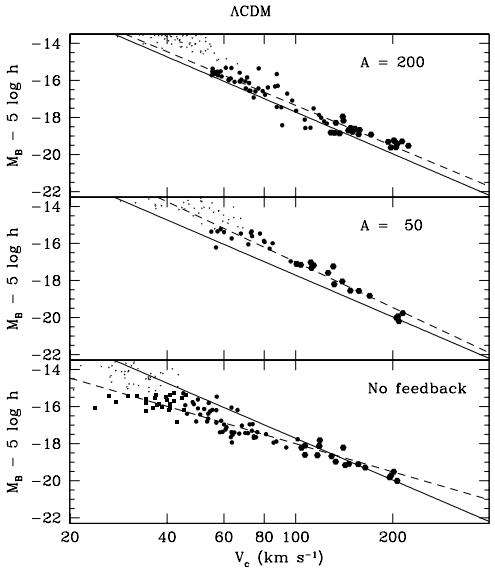

Fig. 6.— (a) Same as Fig 5.(a) but for the ΛCDM model

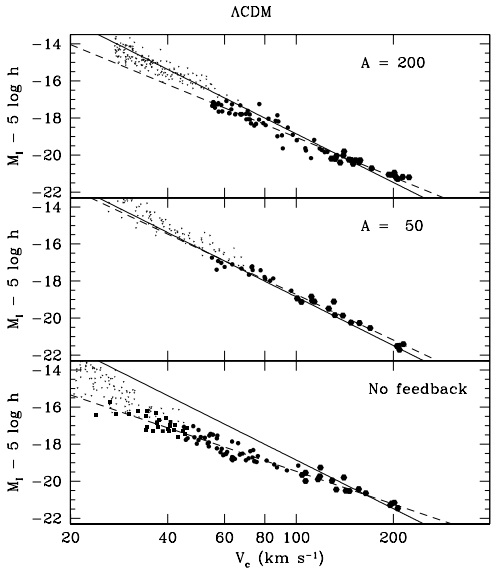

Fig. 6.— (b). Same as Fig 5.(b) but for the ΛCDM model

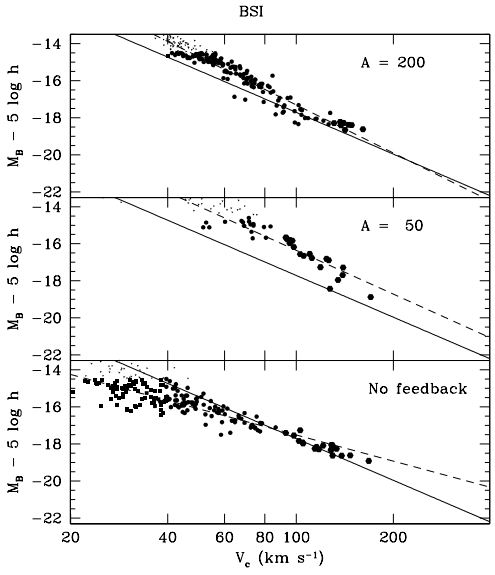

Fig. 7.— (a). Same as Fig 5.(a) but for BSI model

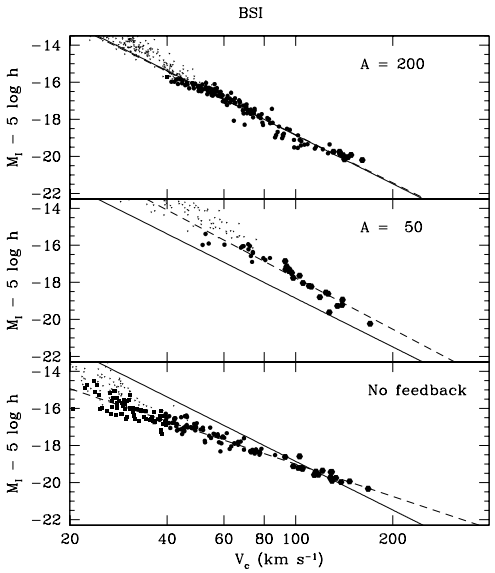

Fig. 7.— Same as Fig 5.(b) but for BSI model.

including those with $M_B > -16$.

To obtain the TF relation in each band considered, we have fit the relation between the log of the circular velocity V_c and the magnitude M in that band according to a formula of the general form

$$M - 5\log h = a\log\left(\frac{V_c}{100\ \mathrm{km\ s^{-1}}}\right) + b \qquad (4)$$

by linear least-squares regression. In order to come closer to the observational situation, the fits include only "bright" galaxies ($M_B < -16$).

Table 3 lists the resulting regression coefficients a and b and the rms scatter ΔM expressed in magnitudes in the B, R, and I spectral band for the observations (Pierce & Tully, 1992) and for the simulated CDM, ΛCDM, and BSI galaxy catalogs. For each scenario, coefficients are computed for each of the supernova feedback parameters. The linear fits are also shown in Figs. 5, 6 and 7.

The results shown in the table and figures illustrate the sensitivity of the TF relation to self-regulating processes affecting star formation in the halos. The different cosmological scenarios correspond to varying characteristic merging histories, while the different values of A correspond to varying supernova feedback.

Before discussing the issue of self-regulation, it is

Table 3: Parameters of linear fits (a, b) and scatter (ΔM), for the magnitude-circular velocity relation in different bands and models. Fits to the observational Tully-Fisher relation (Pierce & Tully 1992) are also shown.

		a			b			ΔM		
Model	Feedback Parameter	B	R	I	B	R	I	B	R	I
Observ.	—	-7.48	-8.23	-8.72	-17.71	-18.47	-18.85	0.34	0.24	0.24
	A=200	-6.08	-6.60	-6.56	-16.21	-17.35	-16.24	0.46	0.35	0.36
CDM	A=50	-7.47	-7.49	-7.49	-15.87	-17.04	-17.63	0.29	0.22	0.21
	A=0	-4.88	-5.47	-5.65	-16.87	-17.81	-18.34	0.59	0.45	0.42
	A=200	-7.28	-7.12	-7.14	-17.68	-18.75	-19.04	0.41	0.33	0.30
ΛCDM	A=50	-8.17	-8.18	-8.18	-16.99	-18.14	-18.72	0.39	0.27	0.25
	A=0	-5.05	-5.65	-5.89	-17.99	-18.92	-19.46	0.48	0.33	0.31
	A=200	-8.60	-8.59	-8.59	-17.31	-18.29	-18.84	0.37	0.28	0.27
BSI	A=50	-7.86	-8.90	-9.20	-16.35	-17.23	-17.75	0.47	0.36	0.33
	A=0	-4.67	-5.48	-5.80	-17.52	-18.44	-18.99	0.45	0.32	0.32

useful to point out some general trends that can be derived from the fits: Particularly noteworthy are the trends in the scatter and zero points. All models have their smallest scatter in the I band, as do observed galaxies, and in all three scenarios the B-band scatter is about 0.10 mag larger than the I-band scatter, in agreement with the observed difference. We also find the same tendency of higher (more negative) zero points for the I band than for the B band. On the other hand, we do not find a systematic increase of the TF slope toward longer wavelengths, at least when feedback from supernovae is switched on. In all models, faint galaxies ($M_B > -16$) seem to be systematically dimmer than predicted by the TF fit for their rotational velocities. This is consistent with results from semi-analytic models (see e.g. CAFNZ, HCFN), although in these models, the departure from linearity is more pronounced for halos with $V_c \leq 150$ km/s than in our simulations.

Concerning the effects of different cosmological scenarios, one sees that the slope of the TF relation is steeper (i.e. more negative) for less evolved models (ΛCDM and BSI). In the CDM model, galaxies with high circular velocity have a lower luminosity than that predicted from the observed TF relation. An explanation for this trend is that in the CDM scenario, galaxies tend to have large star formation rates at relatively early epochs. As a result, these galaxies have already transformed most of their gas into stars, and the remaining gas does not cool fast enough to support a constant SFR, because it is too hot and the density is too low. The net result is a decline in the SFR of these galaxies from $z \lesssim 0.5$ up to the present epoch. A more detailed treatment is given in Elizondo et al., 1998.

Table 3 and the figures show that the slope of the TF relation depends quite strongly on the strength of supernova feedback. For low values of A (i.e. efficient gas reheating and less evaporation of cold clouds), pressure gradients are effective in driving the gas away from the center of halos with low circular velocity (≤ 150 km/s). This results in a decrease in the star formation rate and hence in fainter galaxies. On the other hand, halos with high circular velocity are hardly affected by supernovae feedback, because high-density gas efficiently radiates the energy released by supernova explosions, keeping pressure gradients low. In this regard, our simulations are in good agreement with previous work (Katz et al. 1992, Navarro and White 1994). Therefore, the TF relation is steeper (more negative slope) for simulations with lower A values. For $A = 200$, the more evolved the scenario (CDM versus ΛCDM, and BSI), the less steep the TF relation. A possible explanation is that in evolved scenarios, smaller halos tend to merge after having consumed most of their gas, so that there is a shift toward higher circular velocities without a corresponding increase in luminosity.

A very interesting result concerns the scatter of the TF relation in simulations with $A = 0$ (no heating or evaporation, but with metal enrichment). ΔM is somewhat higher than for simulations with feedback. Nevertheless, it is still comparable with the observa-

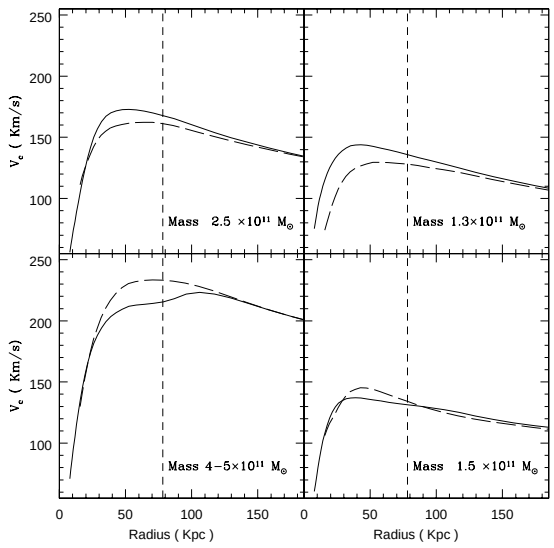

Fig. 8.— Effects of resolution on the circular velocity profile of 4 more massive halos in one of the ΛCDM simulations reported in the paper. The solid line is the circular velocity for the high-resolution simulation (256^3). Dashed lines correspond to the halos found in the same realization that was re-run at lower resolution (128^3). The vertical dotted line represents the limiting radius for these halos according to our galaxy finding algorithm.

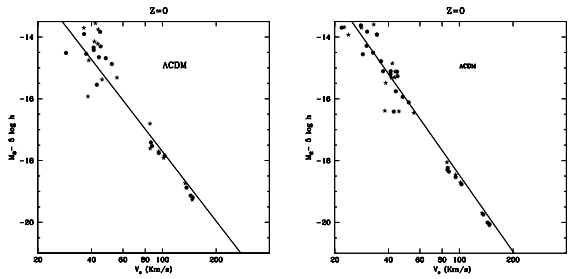

Fig. 9.— Effects of resolution on the TF relation (in B and R bands) for one of the ΛCDM simulations reported in this paper. The solid dots represent galaxies found in the 256^3 simulation (20 kpc resolution). Star points are galaxies found in the same simulation but run with 128^2 cells (40 kpc resolution) and particles. Solid line represents the observational fit to the TF relation (Pierce & Tully 1992).

tional estimates. This seems to imply that the origin of the small scatter in the TF relation cannot be attributed solely to nonlinear feedback processes from supernova explosions. We will discuss this point in § 7. The slope of the TF relation for $A = 0$ is quite similar in all three cosmological models. It is flatter than in simulations with feedback and very different from the observations. However, the luminosities of large circular velocity halos are not strongly affected by turning off feedback.

5. Numerical effects

Previous tests of our numerical simulation code were reported in YK[3]. For the present study, several additional controls and tests were carried out to quantify the effects of numerical resolution on our results. As explained in § 2.1, one of the ΛCDM realizations was simulated at two different resolutions. We can thus study the sensitivity of both the circular velocity estimate and the magnitude assignment to numerical resolution and check for biasing in the slope of the TF relations in different bands.

Fig. 8 shows the circular velocity profiles as a function of radius for the four most massive halos found in the test simulation. The circular velocity estimates at the limiting radius for these halos differ by less than 10% despite the factor of two difference in cell width.

In Fig. 9, we plot magnitudes vs. circular velocities in the B and R bands for the galaxies found in the simulation with 256^3 particles and cells (19.5 kpc resolution, solid dots) and in the 128^3 simulation (39 kpc resolution, asterisks). The effects of resolution on magnitude are more pronounced for low circular velocity halos than for high circular velocity halos. Nonetheless the linear fit to the relation is hardly affected. In the high resolution simulation, we find that ΔM_B is reduced by $\sim 20\%$ and ΔM_R by $\sim 30\%$ as compared with the results for the low-resolution simulation.

From this analysis, we conclude that our star-gas model results in galaxies with properties that are robust with respect to a factor of two change in numerical resolution.

As an independent test of the effects of resolution on the circular velocity profiles of dark halos, one of the CDM realizations was also simulated using the *Adaptive Refinement Tree (ART)* N-body code of Kravtsov, Klypin and Khokhlov (1997). The formal

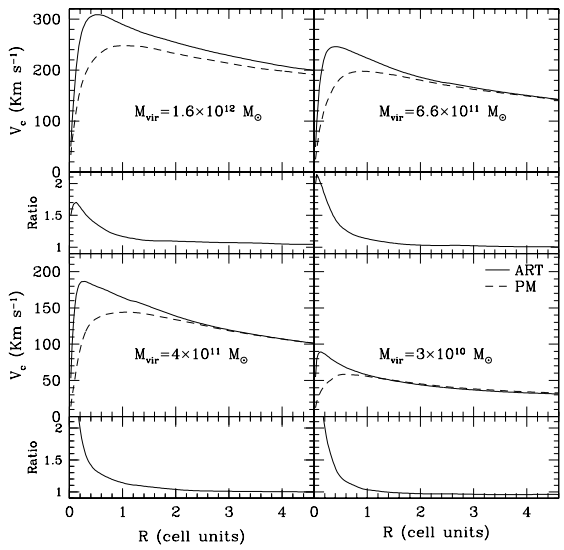

Fig. 10.— Circular velocity profiles as a function of radius (cell units) for four halos found in a CDM realization simulated using two different N-body codes: a high resolution ($\sim 0.2kpc$) ART code (Kravtsov, Klypin & Khokhlov 1997) (solid lines) and our PM N-body code (dashed lines). Lower boxes in each panel show the ratio of the two circular velocity estimates as a function of radius.

resolution of this simulation, at $z = 0$ is $\sim 0.2kpc$. Despite the relatively low resolution of our simulation, the overall structures of dark halos are similar to those of the ART simulation. We have identified the most massive dark halos and computed the velocity profiles, for dark matter only, in both simulations. In Fig 10 we show the results of this comparison for four typical massive halos. As expected, the differences are striking at scales smaller than our cell resolution (39 kpc). However, at the two-cell radius, our circular velocity estimate coincides almost exactly with the high-resolution estimate. The peak of the velocity curve of halos found in the ART simulation is up to a factor of ~ 2 larger than the maximum of the velocity profile from our simulation. Nevertheless, circular velocities are assigned at the two-cell radius, not at the peak, and luminosities are also defined within the two-cell radius for massive galaxies.

6. Luminosity functions

Semianalytical models of galaxy formation have found it very difficult to reconcile the observed zero-point of the TF relation with the overall amplitude of the luminosity function (LF). It has been argued (Frenk et al. 1996) that this problem is related to the overabundance of dark matter halos predicted in all CDM cosmologies. Dark matter simulations indicate that the mass function of galactic halos has a slope of $\alpha \sim -2$ at the low-mass end, which is steeper than any estimate of the observed field galaxy luminosity function. Hydrodynamical simulations such as those reported in this paper and semianalytical models (i.e. CAFNZ) have demonstrated that the faint end of the luminosity function is very sensitive to the combined effects of mergers and supernova feedback.

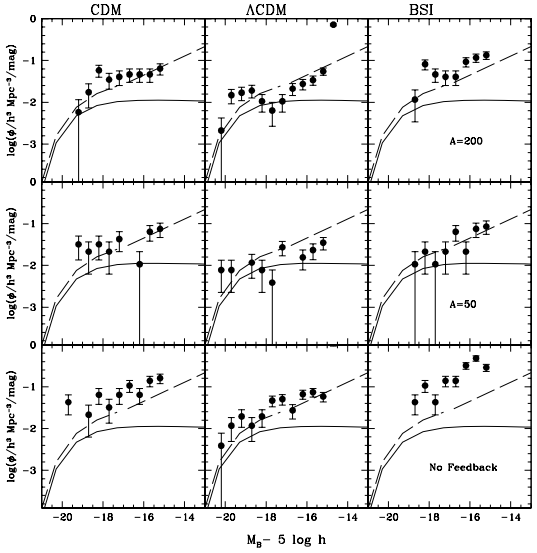

Fig. 11.— Luminosity function (LF) in the B band. Filled circles represent the LF obtained from the numerical galaxies generated in simulations with different feedback parameters (top panels: $A = 200$, central panels: $A = 50$, and bottom panels: no feedback ($A = 0$)). Error bars represent Poisson errors in each magnitude bin. Solid lines are the best-fitting Schechter function from the Stromlo-APM survey (Loveday et al. 1992). Dashed line correspond to the best fit to the LF obtained from ESP galaxy redshift survey (Zucca et al. 1997)

.

In Figs. 11 and 12 we show the luminosity functions (solid circles) in the B and K band estimated from the numerical galaxies generated in the realizations of the three cosmological simulations with different feedback parameters (top panels: $A = 200$, central panels: $A = 50$ and bottom panels: no feedback). Observational estimates for the local luminosity functions are also shown. For the B band, the solid line represents the Schechter function with $\alpha \sim -1$, which best fits the observational data from the Stromlo-APM survey (Loveday et al. 1992). The dashed line shows a more recent estimate of the LF found from the ESO Slice Project (ESP) galaxy redshift survey by Zucca et al. (1997). These authors find a Schechter function with $\alpha = -1.22$ as an acceptable representation of the LF over the entire range of magnitudes $M_B - 5\log h \leq -12.2$. However, their data also suggest the presence of a steepening of the luminosity function for $M_B - 5\log h \geq -16.8$. Such a steepening at the faint end of the LF is well fitted by a power law with slope ~ -1.6. The range of magnitudes of the galaxies in our simulations ($-20 \lesssim M_B \lesssim -15$) allows us to study the faint-end slope of the LF only.

In the K band plots, we show the Schechter functions fitting the most recent observational data in the near infrared band. Solid lines represent the best fit to the Szokoly et al. (1998) survey ($\alpha = -1.27$). Dotted lines are the best fit to the LF obtained by Gardner et al. (1997) ($\alpha = -1.03$). Dashed line corresponds to the best-fit LF obtained by Glazebrook et al. (1995) ($\alpha = -1.04$).

The lack of bright galaxies, due to the small simulated box, precludes drawing conclusions about the observed break at the bright end of the LF. The faint-end slopes of the B-band LF derived from our data are steeper ($\alpha \sim -1.5$ to -1.9, for $-18 \leq M_B \leq -15$) than the estimate of Loveday et al. (1992), but they are in rough agreement with the recent estimates from the ESP survey.

For the K-band, our galaxies have magnitudes much fainter ($-22 \lesssim M_K \lesssim -14$) than those of the near-infrared redshift surveys ($M_K \lesssim -21$). Therefore, our data should be compared with the extrapolation of the best-fitting Schechter functions towards fainter magnitudes. Our data show a clear trend toward a steepening of the slope of the luminosity function at the faint end, in agreement with the recent estimates of Szokoly et al. (1998), as compared with the results of Glazebrook et al. (1995) and Gardner et al. (1997). The slopes for the faint end of the LF from our data are in the range $\alpha \sim -1.2$ to -1.5.

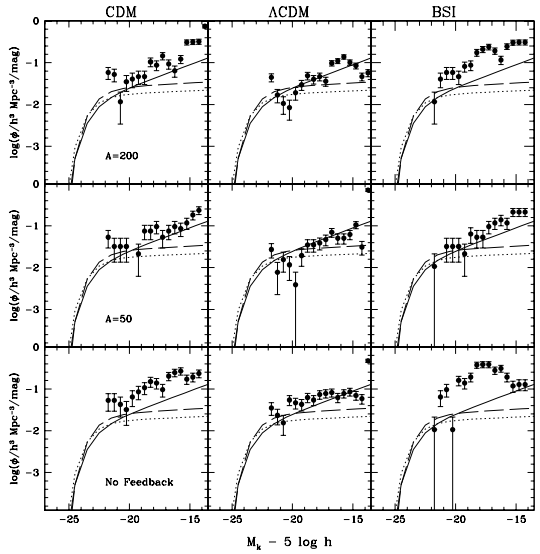

Fig. 12.— Same as in figure 11 but for the K band. Solid line is the best-fitting Schechter function from Szokoly et al. (1998). Dotted line is the best fit to the LF obtained by Gardner et al. (1997). Dashed line corresponds to the best fitting LF obtained by Glazebrook et al. (1995)

.

In view of the dependence of the luminosity function normalization on merging rates and supernova feedback we can explain the higher faint-end BSI LF as follows: In the BSI simulations, galaxies tend to form later than in the ΛCDM or CDM simulations. When supernova feedback is included, it most strongly affects star formation in small galactic halos, which end up fainter, as noted above. The net result is a lower normalization of the luminosity functions for BSI with supernova feedback than without it. Efficient reheating of gas from supernovae (low A) results in a luminosity function with lower normalization than with more evaporation (high A). Again this effect is more pronounced in the BSI simulations, because most of the galactic halos have small potential wells, so gas can more easily escape due to the relative large pressure gradients generated by supernova explosions.

7. Discussion and Conclusions

Using hydrodynamical simulations of galaxy formation with star formation and supernova feedback we have found that it is possible to reproduce the slope, offset, and scatter of the TF - relation. It is quite intriguing to ask which elements of the approach are essential for the different parts of the relation: In simulations without supernova feedback (energy input and mass transfer from supernova is switched off, but metal enrichment is left on), the slope of the resulting TF - relation is too shallow $a \sim -5$, or $L \propto V_c^2$, with nearly equal zero-point in all three scenarios (cf. Table 3). This slope agrees with estimates from the Press-Schechter theory (Cole and Kaiser, 1989) which incorporate cooling but ignore feedback and assume that all cold gas is converted into stars.

According to our results, the slope of the TF relation depends quite strongly on the level of feedback. The effects of supernova feedback are certainly much less significant for galaxies with $V_c \gtrsim 150$ km s^{-1} (cf. Figs 5–7) in fairly good agreement with previous results (e.g. Navarro & White 1993; Katz et al. 1996). Supernova feedback tends to have a stronger effect on star formation in low circular velocity halos. Hence supernova feedback causes a steepening of the slope, because low-mass halos become fainter while the luminosity of massive halos remains basically unchanged. This feature of the TF relation is the common to the three cosmological scenarios considered here.

The slope of the TF is the same for all photometric bands when feedback is considered, while for simulations without feedback, the TF-slope is steeper for redder wavelengths. These results suggest that the observed passband dependence of slope of the TF relation should not be attributed to different star-formation histories of galaxies. Although corrections for dust extinction have been made in the analysis of observations (Pierce and Tully, 1992), these corrections are rather difficult to estimate and hence uncertain. Dust extinction could well be responsible for the differences between the B-band and I-band TF slopes. Moreover, recent semianalytical models which include dust extinction also find a varying slope of the TF with wavelength (Somerville & Primack 1998; Firmani & Avila-Reese 1998). An important extension of the present framework will be to incorporate the effects of dust extinction including a refined model for the metal production of stars.

Another important ingredient of the TF relation is the intrinsic scatter. As we have already mentioned, a long standing question concerns whether this scatter is a consequence of cosmological conditions, or whether it is rather produced by the nonlinear physical processes associated with star formation that occur in the interior of halos. Interestingly, the TF scatter does not change much as the supernova feedback parameter is varied, as long as feedback is not turned off completely (all SN energy radiated away immediately). However, the scatter in simulations with feedback turned off is about double the observed TF scatter. Feedback processes tend to reduce this scatter, because they are coupled to merging rates and dynamical evolution. For instance, the rms scatter in BSI simulations is hardly affected by feedback, while in CDM simulations, the rms scatter with feedback is half that of simulations without feedback. Hence, the idea of Eisenstein & Loeb (1996) that small TF scatter is related to nonlinear feedback mechanisms could indeed be correct, but some nonlinear element in addition to supernova feedback must play an essential role in reducing it.

In a recent paper, Somerville & Primack (1998) have carefully compared different semianalytical model predictions for the TF scatter and slope. They conclude that the predictions are sensitive to different assumptions concerning supernovae feedback. In particular, the "Durham semianalytical model" (CAFNZ) has a feedback model that is too strong, resulting in a nonlinear TF relation at low circular velocities. The "Munich model" (KWG) has a milder feedback model and consequently, it gets a flatter slope for the TF, in agreement with our numerical results. Avila-Reese, Firmani and Hernández (1998) use a different semianalytical approach for the virialization of baryonic material in rather isolated (mass accretion dominates over major mergers) dark matter halos, without gas outflow from the disk. They find a scatter in the TF relation which is somewhat higher (within a factor of 2) than in observations (Pierce & Tully 1992), in fairly agreement with what we find in our simulations with no feedback. In these semianalytical models, the scatter in the TF relation can be traced back to the scatter in the mass accretion histories of halos of similar mass (e.g. Avila-Reese 1998).

In this regard, it is interesting to compare the redshift evolution of the star formation rate for some of our halos with predictions of semianalytical calculations, kindly provided by V. Avila-Reese. In Fig 7

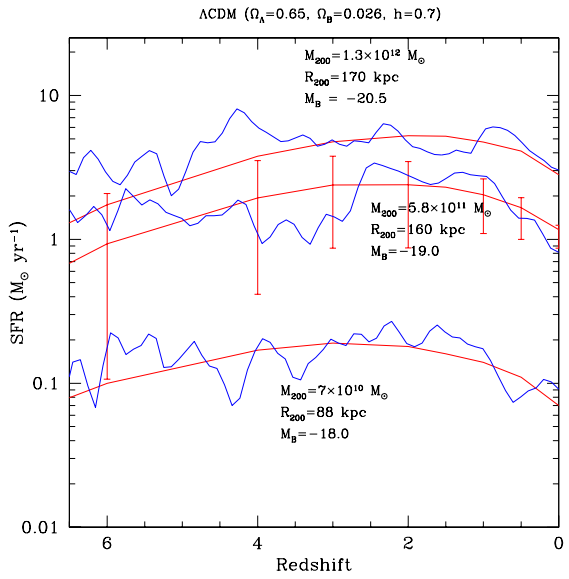

Fig. 13.— Comparison of the redshift evolution of the Star Formation Rate for three different halos in one of our ΛCDM simulation (thin solid lines), with averaged predictions from semianalytical galaxy formation models (Firmani & Avila-Reese 1998). The error bars correspond to the maximum and minimum values of the SFR in the Montecarlo realizations of mass accretion histories for the corresponding halo.

we show the star formation rate (SFR) as a function of redshift for three halos of different mass in one of our ΛCDM simulations. The thick solid lines represent the average SFR for halos of same virial mass, computed by means of the semianalytical model developed by Firmani and Avila-Reese (1998). The error bars represent the maximum and minimum SFR values at different redshifts for the 2000 Monte Carlo realizations of mass accretion histories for this halo. This semianalytical model of formation of disk galaxies includes a simplified hydrodynamical treatment of the gas and models the effects of supernovae on the cold gas clouds as an increase in their turbulent motion. This model differs from our picture of cloud evaporation, but it nonetheless provides an effective feedback mechanism. The scatter in the TF relation for these models is somewhat higher than the one we obtain in the simulations. However, the overall agreement between these semianalytical calculations and our simulations is remarkable. (See Firmani & Avila-Reese 1998 for further details).

The answer to the question of whether the scatter of TF is a consequence of cosmological conditions, or rather results from nonlinear processes associated with star formation in the dark halos, could well be: *The scatter of the TF is due to a combination of effects in which nonlinearities of several kinds play essential roles.* The intrinsic scatter that results in the formation and virialization of galactic halos is reduced when additional nonlinear processes due to the supernovae feedback loop are taken into account. Those semianalytical models with a highly nonlinear model of the baryonic physics tend to find small scatter. As a general rule, numerical simulations that self-consistently incorporate gravity, hydrodynamics and feedback effects will include more nonlinearity than simpler approximations. Hence, it is not surprising that a lower scatter in the TF relation is found in simulations than in semianalytical model predictions.

We have also estimated the luminosity functions in B and K bands from the simulated galaxies. The relatively small volumes of our present simulations preclude a reliable estimate of the full LF in the different cosmological scenarios, since as explained earlier bright galaxies are undersampled or completely absent due to the lack of high-density regions. With this caveat in mind, we have compared the number density of faint objects with observations. The faint end of the LF is very much affected by supernova feedback. This is especially important for the less evolved BSI simulations, in which a high number density of faint objects is found. In all simulations, we systematically find steeper slopes for the B band luminosity functions than the estimates from the Stromlo-APM survey (Loveday et al. 1992), but they are compatible with recent estimates from the ESO Slice Project (Zucca et al. 1997).

Despite possible uncertainties in the determination of the LF from our simulations, we can conclude that, with an adequately chosen value for the feedback parameter, our model of self-regulating star formation can reproduce the correct TF zero point and the right number density of objects, at least for the ΛCDM model. For the CDM simulations, halos tend to have a lower luminosities for a given circular velocity, so the zero point of the TF relation is incompatible with observations, while for the BSI model, the low normalization of the spectrum produces far too many faint objects. The number of objects can be reduced by assuming a small value for the feedback parameter ($A = 50$), which means a large thermal reheating.

In this case, the galaxies are fainter and the TF zero point is not compatible with the observed one.

We saw in Section 5 that our results are fairly robust with respect to changes in numerical resolution and details of the galaxy finding scheme. Doubling the resolution did not significantly affect the TF relation, although some individual galaxy colors were shifted. As resolution is further increased, we expect that some adjustment of parameters in our modeling of processes occurring below the limits of resolution will be required.

A final conclusion of this paper is that self-regulation of star formation such as supernova feedback and hyrodynamical processes must play an essential role in explaining the observational properties of galaxies.

We wish like to thank Claudio Firmani and Vladimir Avila-Reese for helpful discussions and for providing us with comparisons from their semianalytical calculations. We would also like to thank Andrey Kravtsov for performing one of our CDM realizations using the ART code and computing the velocity profiles. This work has been partially supported by the DGICyT (Spain) under project number PB93-0252. R.K. gratefully acknowledges a fellowship of the DFG (Germany) during part of this work.

REFERENCES

Avila-Reese, V., 1998, Ph. D. Thesis, UNAM

Avila-Reese, V., Firmani, C., & Hernández, X., 1998, ApJ (in press), astro-ph/9710201

Bruzual, G., & Charlot, S., 1993, ApJ, 405, 538

Cen, R., & Ostriker, J. P., 1992, ApJ, 399, 113

Cole, S., & Kaiser, N., 1989 MNRAS, 237, 1127

Cole, S., Aragón-Salamanca, A., Frenk, C.S., Navarro, J.F., & Zepf, S.E., 1994, MNRAS, 271, 781 (CAFNZ)

Colella, P., & Woodward, P. R., 1984, J.Comp.Phys, 54, 174

Courteau, S., 1997, AJ, 114, 2402

Eisenstein, D.J., & Loeb, A., 1996, ApJ, 459, 432

Elizondo, D., 1996, Ph. D. Thesis, Universidad Autónoma de Madrid

Elizondo, D., Yepes, G., Kates, R., & Klypin, A., 1998 (submitted to New Astronomy)

Evrard, A., Summers, F, & Davis, M., 1994, ApJ, 422, 11

Firmani, C., & Avila-Reese, V., 1998, preprint, astro-ph/9803090

Freeman, K.C., 1970, ApJ, 160, 811

Frenk, C.S., Baugh, C. M., Cole, S., & Lacey, C., 1996, astro-ph/9612109

Gardner, J.P., Sharples, R.M., Frenk, C.S., & Carrasco, B.E., 1997, ApJ, 480, L99

Giroux, M., & Shapiro, P. 1986, ApJS, 102, 191

Glazebrook, K., Peacock, J.A., Miller, L., & Collins, C.A., 1995, MNRAS, 275, 65

Heyl, J.S., Cole, S., Frenk, C.S. & Navarro, J.F., 1995, MNRAS, 274, 755 (HCFN)

Kates, R., Müller, V., Gottlöber, S., Mücket, J.P., & Retzlaff, J. 1995, MNRAS, 277, 1254

Katz, N, 1992, ApJ, 391, 502

Katz, N., Hernquist, L., & Weinberg, D.H., 1992, ApJ, 399, 109

Katz, N., Weinberg, D.H, & Hernquist, L., 1996, ApJS, 105, 19

Kauffmann, G., White, S.D.M., & Guiderdoni, B., 1993, MNRAS, 264, 201 (KWG)

Kravtsov, A., Klypin, A & Khokhlov, A., 1997, ApJS 111 73

Lacey, C., & Cole, S., 1993, MNRAS, 262, 627

Loveday, J., Peterson, B. A., Efstathiou G., & Maddox, S.J., 1992, ApJ, 390, 338

Marzke, R.O., Huchra, J.P., & Geller, M.J., 1994 ApJ, 428, 43

McKee, C.F. & Cowie, L.L., 1977, ApJ, 215, 213

Navarro, J.F., & White, S.D.M., 1994, MNRAS, 267, 401

Persic, M., Salucci, P., & Stel, C., 1996, MNRAS, 281, 27

Petitjean, P., Mücket, J, & Kates, R. 1995, A&A, 295, L9

Pierce, M.J. & Tully, R.B., 1988, ApJ, 330, 579

Pierce, M.J. & Tully, R.B., 1992, ApJ, 387, 47

Steinmetz, M. & Müller, E., 1994, A&A281, 97

Somerville, R.C., & Primack, J. R., 1998, preprint, astro-ph/9802268

Szokoly, G.P., Subbbarao, M.U., Connolly. A.J., & Mobasher, B., 1998, ApJ, 492, 452

Strauss, M.A., & Willick, J.A., 1995, Phys. Rep., 261, 271

Tully, R.B., & Fisher. J.R., 1977, A&A, 54, 661

Yepes, G., Kates, R., Klypin, A. & Khokhlov, A., 1995, Proceedings of the XVth Recontres des Moriond *"Clustering in the Universe"*. S. Maurogordato, C. Balowski, C. Tao, & J. Trán Thanh Ván (eds), pp. 403-407

Yepes, G., Kates, R., Khokhlov, A., & Klypin, A., 1997, MNRAS, 284, 235 (YK^3)

Zucca, E., et al., 1997, A&A, 326, 477

This 2-column preprint was prepared with the AAS LaTeX macros v4.0.